2017

Strain Sensor Based on Grourd-Shaped Single-mode-multimode-single-mode Hybrid Optical Fibre Structure

Ke Tian
Harbin Engineering University

Gerald Farrell
Technological University Dublin, gerald.farrell@tudublin.ie

Xianfan Wang
Harbin Engineering University

See next page for additional authors

Recommended Citation

Tian, K. et al (2017). Strain sensor based on gourd-shaped single-mode-multimode-single-mode hybrid optical fibre structure. *Optics Express*, vol. 25, no. 16, pg. 18885. doi:10.1364/OE.25.018885

Research Article | Vol. 25, No. 16 | 7 Aug 2017 | OPTICS EXPRESS 18885
Optics EXPRESS

Strain sensor based on gourd-shaped single-mode-multimode-single-mode hybrid optical fibre structure

KE TIAN,[1] GERALD FARRELL,[2] XIANFAN WANG,[1] WENLEI YANG,[1] YIFAN XIN,[1] HAIDONG LIANG,[1,3] ELFED LEWIS,[4] AND PENGFEI WANG[1,2,*]

[1]*Key Laboratory of In-fiber Integrated Optics of Ministry of Education, College of Science, Harbin Engineering University, Harbin 150001, China*
[2]*Photonics Research Centre, Dublin Institute of Technology, Kevin Street, Dublin 8, Ireland*
[3]*Hands and Feet Microsurgery, the Second Hospital of Dalian Medical University, Dalian 116023, China*
[4]*Optical Fibre Sensors Research Centre, Department of Electronic and Computer Engineering, University of Limerick, Limerick, Ireland*
**pengfei.wang@dit.ie*

Abstract: A fibre-optic strain sensor based on a gourd-shaped joint multimode fibre (MMF) sandwiched between two single-mode fibres (SMFs) is described both theoretically and experimentally. The cladding layers of the two MMFs are reshaped to form a hemisphere using an electrical arc method and spliced together, yielding the required gourd shape. The gourd-shaped section forms a Fabry-Perot cavity between the ends of two adjacent but non-contacting multimode fibres' core. The effectiveness of the multimode interference based on the Fabry-Perot interferometer (FPI) formed within the multimode inter-fibre section is greatly improved resulting in an experimentally determined strain sensitivity of –2.60 pm/με over the range 0—1000 με. The sensing characteristics for temperature and humidity of this optical fibre strain sensor are also investigated.

OCIS codes: (060.2370) Fiber optics sensors; (050.2230) Fabry-Perot; (230.7370) Waveguides.

References and links

1. L. Han, S. Liang, J. Xu, L. Qiao, H. Zhu, and W. Wang, "Simultaneous Wavelength-and Mode-Division (De) multiplexing for High-Capacity On-Chip Data Transmission Link," IEEE Photonics J. **8**, 1–10 (2016).
2. P. Wang, Y. Semenova, and G. Farrell, "Temperature dependence of macrobending loss in all-fiber bend loss edge filter," Opt. Commun. **281**(17), 4312–4316 (2008).
3. W. S. Mohammed, P. W. E. Smith, and X. Gu, "All-fiber multimode interference bandpass filter," Opt. Lett. **31**(17), 2547–2549 (2006).
4. Y. Zhao, P. Wang, R. Lv, and Y. Yang, "Temperature Sensing Characteristics Based on Up-Taper and Single Mode–Multimode Fiber Structure," IEEE Photonics Technol. Lett. **28**(22), 2557–2560 (2016).
5. K. Tian, Y. Xin, W. Yang, T. Geng, J. Ren, Y.-X. Fan, G. Farrell, E. Lewis, and P. Wang, "A Curvature Sensor Based on Twisted Single-Mode–Multimode–Single-Mode Hybrid Optical Fiber Structure," J. Lightwave Technol. **35**(9), 1725–1731 (2017).
6. D.-P. Zhou, L. Wei, W.-K. Liu, and J. W. Y. Lit, "Simultaneous strain and temperature measurement with fiber Bragg grating and multimode fibers using an intensity-based interrogation method," IEEE Photonics Technol. Lett. **21**(7), 468–470 (2009).
7. J. An, Y. Jin, M. Sun, and X. Dong, "Relative humidity sensor based on SMS fiber structure with two waist-enlarged tapers," IEEE Sens. J. **14**(8), 2683–2686 (2014).
8. P. Wang, G. Brambilla, M. Ding, Y. Semenova, Q. Wu, and G. Farrell, "High-sensitivity, evanescent field refractometric sensor based on a tapered, multimode fiber interference," Opt. Lett. **36**(12), 2233–2235 (2011).
9. H. Dong, L. Chen, J. Zhou, J. Yu, H. Guan, W. Qiu, J. Dong, H. Lu, J. Tang, W. Zhu, Z. Cai, Y. Xiao, J. Zhang, and Z. Chen, "Coreless side-polished fiber: a novel fiber structure for multimode interference and highly sensitive refractive index sensors," Opt. Express **25**(5), 5352–5365 (2017).
10. Q. Wang, G. Farrell, and W. Yan, "Investigation on single-mode–multimode–single-mode fiber structure," J. Lightwave Technol. **26**(5), 512–519 (2008).
11. Q. Wu, Y. Semenova, B. Yan, Y. Ma, P. Wang, C. Yu, and G. Farrell, "Fiber refractometer based on a fiber Bragg grating and single-mode-multimode-single-mode fiber structure," Opt. Lett. **36**(12), 2197–2199 (2011).

#297357 https://doi.org/10.1364/OE.25.018885
Journal © 2017 Received 5 Jun 2017; revised 15 Jul 2017; accepted 17 Jul 2017; published 26 Jul 2017

Optics EXPRESS

12. Y. Zhao, L. Cai, X.-G. Li, and F.-C. Meng, "Liquid concentration measurement based on SMS fiber sensor with temperature compensation using an FBG," Sens. Actuators B Chem. **196**, 518–524 (2014).
13. S. W. James, M. L. Dockney, and R. P. Tatam, "Simultaneous independent temperature and strain measurement using in-fibre Bragg grating sensors," Electron. Lett. **32**(12), 1133–1134 (1996).
14. H. Zeng, T. Geng, W. Yang, M. An, J. Li, F. Yang, and L. Yuan, "Combining two types of gratings for simultaneous strain and temperature measurement," IEEE Photonics Technol. Lett. **28**(4), 477–480 (2016).
15. X. Dong, H. Y. Tam, and P. Shum, "Temperature-insensitive strain sensor with polarization-maintaining photonic crystal fiber based Sagnac interferometer," Appl. Phys. Lett. **90**(15), 151113 (2007).
16. M. Sun, B. Xu, X. Dong, and Y. Li, "Optical fiber strain and temperature sensor based on an in-line Mach–Zehnder interferometer using thin-core fiber," Opt. Commun. **285**(18), 3721–3725 (2012).
17. Y. Zhao, M. Chen, R. Lv, and F. Xia, "In-fiber rectangular air fabry-perot strain sensor based on high-precision fiber cutting platform," Opt. Commun. **384**, 107–110 (2017).
18. A. M. Hatta, Y. Semenova, Q. Wu, and G. Farrell, "Strain sensor based on a pair of single-mode-multimode-single-mode fiber structures in a ratiometric power measurement scheme," Appl. Opt. **49**(3), 536–541 (2010).
19. Y. Liu and L. Wei, "Low-cost high-sensitivity strain and temperature sensing using graded-index multimode fibers," Appl. Opt. **46**(13), 2516–2519 (2007).
20. P. Xian, G. Feng, and S. Zhou, "A Compact and Stable Temperature Sensor Based on a Gourd-Shaped Microfiber," IEEE Photonics Technol. Lett. **28**(1), 95–98 (2016).
21. W. S. Mohammed, A. Mehta, and E. G. Johnson, "Wavelength tunable fiber lens based on multimode interference," J. Lightwave Technol. **22**(2), 469–477 (2004).
22. L. B. Soldano and E. C. M. Pennings, "Optical multi-mode interference devices based on self-imaging: principles and applications," J. Lightwave Technol. **13**(4), 615–627 (1995).
23. C. M. Miller, *Optical fiber splices and connectors: theory and methods* (Marcel Dekker Inc, 1986), Vol. 10.
24. M. Han and A. Wang, "Mode power distribution effect in white-light multimode fiber extrinsic Fabry-Perot interferometric sensor systems," Opt. Lett. **31**(9), 1202–1204 (2006).
25. M. Han and A. Wang, "Exact analysis of low-finesse multimode fiber extrinsic Fabry-Perot interferometers," Appl. Opt. **43**(24), 4659–4666 (2004).
26. E. Li, "Temperature compensation of multimode-interference-based fiber devices," Opt. Lett. **32**(14), 2064–2066 (2007).
27. A. Zhou, B. Qin, Z. Zhu, Y. Zhang, Z. Liu, J. Yang, and L. Yuan, "Hybrid structured fiber-optic Fabry-Perot interferometer for simultaneous measurement of strain and temperature," Opt. Lett. **39**(18), 5267–5270 (2014).

1. Introduction

In recent years, single-mode-multimode-single-mode (SMS) hybrid fibre structures have been intensively investigated. They can be employed as the basis of many photonic devices, in a wide range of applications in telecommunications including wavelength division multiplexing [1], edge and bandpass splitters [2, 3]. SMS fibre structures have also been developed and adapted for a wide range of sensing applications, e.g., temperature [4], curvature [5], strain [6], humidity [7] and refractive index (RI) [8, 9]. The SMS structure offers many advantages such as a compact form-factor, a natural immunity to external electromagnetic interference, low cost and ease of fabrication, etc. A fundamental reason why an SMS fibre structure can be adapted to suit different applications is its inherent simplicity and its use of multimode interference (MMI) as its underlying operating principle. A theoretical analysis of the SMS fibre structure is described in [10]. In addition, an SMS fibre structure exhibits excellent compatibility with other photonic devices and structures e.g. it can be easily connected to other optical fibre structures (by fusion splicing) with a great degree of flexibility allowing for the achievement of enhanced sensor performance, for example higher sensitivity or an implementation of multi-parameter measurement [11, 12].

Optical fibre based strain sensors have attracted significant research attention and have been widely investigated for applications in engineering fields such as oil and gas exploration and structural health monitoring (SHM). Initially, optical fibre strain sensors were predominantly based on fibre grating structures including fibre Bragg gratings (FBG) [13] and long-period gratings (LPG) [14]. However, in these grating based devices, both temperature and strain can influence the wavelength shift. This significant temperature-strain cross-sensitivity has proved to be a major obstacle in practical applications. In recent years, optical fibre strain sensors based on interferometers have become increasingly popular. Examples include the Sagnac interferometer [15], Mach-Zehnder interferometer (MZI) [16], Fabry-Perot interferometer (FPI) [17] and MMI [18, 19]. Optical fibre strain sensors based on

Optics EXPRESS

MMI offer the advantages of potentially lower fabrication cost, higher sensitivity while being more mechanically robust compared with the other interference based devices. An SMS (using a step-index MMF) fibre structure strain sensor based on intensity variation monitoring has been proposed in [18], for which the measurement scheme is relatively complicated. Graded-index (GI) MMF has also been used to perform strain sensing and proved to have higher strain sensitivity [19]. However, this type of structure is not compact and has high fabrication costs given that it is necessary to utilize a graded-index MMF of up to 1.8 m length. Thus there is a need for a strain sensor based on MMI that is compact, low cost and which offers high sensitivity. The composite interferometer structure proposed in this article provides a possible solution to this problem.

In this letter, an optical fibre strain sensor based on single-mode-gourd-shaped multimode-single-mode (SGMS) fibre structure is proposed and investigated theoretically and experimentally. A gourd-shaped spliced MMF can be realized through a relatively simple fabrication process using only a fusion splicer. By careful control of the arc energy and duration, it is possible to form a hemispherical surface on the ends of each of the two MMF sections, with the hemispherical sections subsequently fused together carefully to form a "gourd" shaped structure. The MMF gourd section is then inserted and fused between two standard SMFs to constitute the finished device. The schematic configuration of the proposed SGMS fibre structure is shown in Fig. 1. The gourd-shaped section forms a Fabry-Perot cavity formed between the ends of the two adjacent but non-contacting cores of the multimode fibres. The composite interference originating from the combination of MMI and the FPI results in enhanced strain sensitivity for the fabricated SGMS fibre structure. The potential cross sensitivity of temperature and humidity to strain are also investigated. The experimental results (Section 4) show that this sensor has a high strain sensitivity and superior stability. The attractive properties of this novel device mean that it has real potential for use for strain measurement in structure health monitoring and other fields.

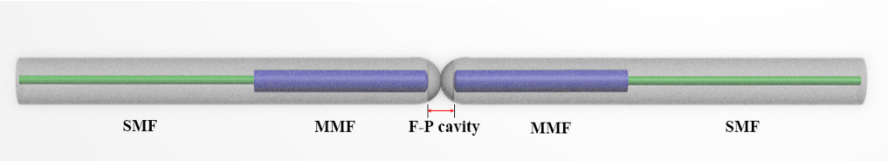

Fig. 1. Schematic of a gourd-shaped spliced SMS fibre structure.

2. Device fabrication

The fabrication process of the SGMS fibre structure is simple and requires only the use of a standard fusion splicer (Fujikura 62S). The vital step is the fabrication of the gourd-shaped MMF section. In this case the electrical arc method is adopted to reshape the vertically cleaved end of the MMF to form a hemisphere. Two MMFs (AFS50/125Y) with 1 cm length each were placed on aligned holding stages, and the electrical arc discharge of the splicer was used to form the cladding of each of the MMFs' ends into a smooth hemisphere with the help of surface tension as the glass becomes molten for a short time as a result of the arc. The single-mode (SM) fusion program was used to control the discharge [20], the arc power and discharge time were 100 a.u. and 200 ms, respectively. It is worth noting that the choice of core radius of the MMF is important. A value that is too large will result in melting of the cladding of the MMFs and it would not be possible to cover the entire fibre's radial profile and hence it is not possible to form an effective Fabry-Perot cavity. For instance, the standard MMF AFS105/125Y (with a core/cladding diameter of 105/125 μm) was found to be unsuitable for this reason, and hence the AFS50/125Y MMF (for which the core/cladding diameter is 50/125 μm) was chosen as the MMF section in this investigation. The next step is to ensure that the two hemispheric ends were correctly aligned with the help of the enlarged view of the fiber ends provided by the view screen of the fusion splicer and are spliced

Optics EXPRESS

together at their equators (which are also the meridional axes of the two fibres involved) employing the manual operation program of the splicer. Finally, this gourd-shaped joint MMF structure was sandwiched between two standard single-mode fibres (SMF-28) hence completing the sensor fabrication. The microscope image of the resulting SGMS fibre structure is presented in Fig. 2. Several essential feature sizes were measured from Fig. 2(a) and Fig. 2(b). The waist diameter D_1 is 65.5 ± 0.5 μm, the distance between two cores L_1 is 110 ± 0.5 μm, and the two microspheres' maximal diameter D_2 is 146.5 ± 0.5 μm, the length of total gourd-shaped structure L_2 is 360 ± 0.5 μm. The surface of the post-splice gourd-shaped section is smooth which ensures that it has minimal evanescent field loss and measurement noise.

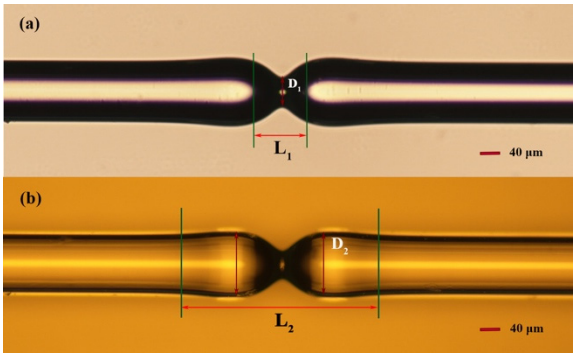

Fig. 2. Optical microscopic image of the gourd-shaped spliced MMFs (a) transmission light; (b) reflected light.

3. Principle and analysis

A schematic diagram is shown in Fig. 3 as a means to illustrate the light propagation in the SGMS fibre structure. An approximated guided-mode propagation analysis method was used to analyze the electric field distribution. Several assumptions were initially employed, i.e. the core of SMF and MMF are assumed to be ideally aligned, there is no vertical offset along the central axis between the two hemispherical structures, the gourd-shaped F-P cavity was assumed to be a common rectangular cavity (in the plan view) and there is no light energy leaked from this cavity.

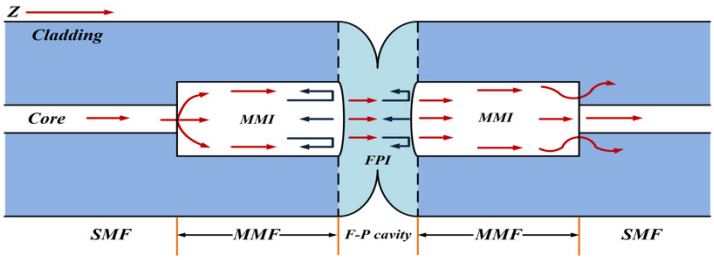

Fig. 3. Schematic diagram of the light transmitted in the SGMS fibre structure.

As shown in Fig. 3, the light is transmitted through the SMF-MMF-F-P cavity-MMF-SMF in spatial sequence. The input radial field distribution was assumed to be Gaussian with a field distribution of E(r,0) due to the radially symmetric characteristic of the circular fundamental mode of the input SMF. When the input light launches into the MMF, only the LP_{0m} modes of the linearly polarized (LP) modes can be efficiently excited due to the circular symmetry of the input field and an ideal alignment of the SMF and MMF as assumed above [21]. For a step-index MMF, the excited mode number of LP_{0m} can be calculated as [10]:

Optics EXPRESS

$M \approx V/\pi$, where $V = \{2\pi/\lambda\}\frac{d}{2}\sqrt{n_{co}^2 - n_{cl}^2}$, d is the diameter of the MMF core, n_{co} and n_{cl} are the refractive index values of MMF core and cladding respectively and λ is the free space wavelength. As the light propagates axially in the MMF section, the field distribution at a propagation distance z can be calculated by [22]:

$$E(r,z) = \sum_{m=1}^{M} c_m F_m(r) \exp(i\beta_m z) \tag{1}$$

where c_m is the excited coefficient of each mode, $F_m(r)$ is the field profile of LP_{0m} and β_m is the propagation constant of each eigenmode.

When the light arrives at the F-P cavity, which is also the first interface between the end of the multimode fibres' core and the hemispherical cladding glass, the total electric field for the light propagating along the z direction can be calculated by a superposition of all M guided modes, which can be written as [23]:

$$E_{total} = \sum_{m=1}^{M} p_m F_m(r) \exp(-j\beta_m z)\hat{e}_m = \sum_{m=1}^{M} |p_m| \exp(j\varphi_{pm}) F_m(r) \exp(-j\beta_m z)\hat{e}_m \tag{2}$$

where e_m is a unit vector representing the polarization of the mode and p_m is the complex magnitude of the mth mode representing the modal distribution in the fibre. At this interface, part of the light energy is reflected back to the input MMF, and the remaining field is transmitted through the F-P cavity. The light is partially reflected at the two internal surfaces of the F-P cavity, but in practice the reflections at these surfaces are weak, given the small refractive index differences, and therefore multiple reflections within the F-P cavity can be ignored [24]. Within the cavity, considering the z direction only, the light injected from the input MMF into the cavity is subject to F-P interference due to the presence of the F-P cavity. It is well established that multiple modes can be excited in MMF as mentioned before, and these excited multiple modes that exist in the cavity cause the F-P interference to be a result of a multiple interference based light interactions. For the transmitted multiple modes, each mode corresponds to a different effective reflectivity $r(L)$ of the F-P cavity which also depend on the cavity length L. Therefore, the eventual field transmitted within F-P cavity can be expressed as:

$$E' = \sum_{m=1}^{M} p_m r_m(L) F_m(r) \exp(-j\beta_m z)\hat{e}_m \tag{3}$$

note that this result is based on the assumption of an approximately rectangular cavity and neglects any light power loss in the F-P cavity as previously stated. When the light enters into second MMF section, each mode is associated with its own different phase value and MMI occurs again. Hence a composite interference pattern based on MMI and FPI is established. Ultimately, a portion of light from the MMF is coupled into the core of the output SMF while the remainder is coupled into the cladding and excites the cladding mode. For the description of the electric field of a particular mode, a more specific and detailed theoretical analysis is available in [25].

Based on the above theoretical analysis, a numerical simulation based on the Beam Propagating Method (BPM) has been used to describe the spatial optical intensity distribution. The simulation conditions involve a mesh size for the X, Y and Z directions of 0.1 μm, 0.1 μm and 1 μm, respectively and the boundary condition in the model adopted is a perfectly matched layer (PML) condition. The simulation parameters that have been used are: the length of both MMFs is 1 cm with a core refractive index 1.4446 and 1.4271 in the cladding. For the gourd-shaped section, the waist diameter D_1' is 70 μm and the distance between two cores L_1' is assumed to be 200 μm. The simulated optical field intensity

Optics EXPRESS

distribution result is presented in Fig. 4 from which it is clear that a regular light transmission pattern occurs as result of MMI within the MMF section. When the light is transmitted through the F-P cavity (the white dashed line in Fig. 4 indicates the start position of the F-P cavity), only a small fraction of the transmitted light intensity is leaked to the external regions ($r > D_1'/2$) and most of the light intensity is transmitted into the second MMF section, which also demonstrates the rationality of the assumption previously adopted. The leaked light is mainly composed of high order modes that are excited and transmitted in the MMF, but a portion of the high order modes become leaky modes due to the gourd-like shape of the joint section between the two MMFs. It is worth noting that leaky modes occurring within the MMF joint section are considered a source of interference for strain measurement since they are capable of interacting with the external environment. Therefore further research into the optimization of the joint fabrication process to minimize leaky modes is needed and is underway.

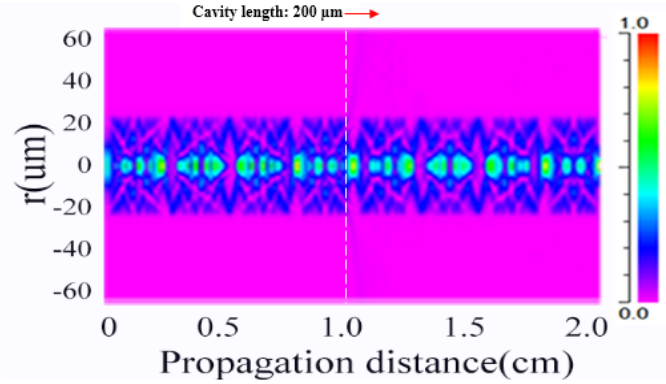

Fig. 4. Simulated optical field intensity distribution within an SGMS fibre structure at a wavelength of 1550 nm using a BPM.

4. Experiment and discussion

The experimental setup for measuring strain using the SGMS fibre structure is illustrated in Fig. 5. A supercontinuum source (SCS, YSL SC-series, China) and a high-resolution (20 pm) optical spectrum analyzer (OSA, YOKOGAWA AQ6370D, Japan, operation wavelength range: 600—1700 nm) were used as the input source and optical signal interrogator, respectively. The sample was placed and fixed on the centre of two electrical translation stages, which can be accurately controlled to actuate motion in the axial direction (shown by arrows in Fig. 5) of the fibre using an electrical displacement controller and hence allow varying axial tensile stress to be applied on fibre structure according to a standard strain calculation formula [26]:

$$\Delta\varepsilon=\frac{\Delta L}{L} \tag{4}$$

where L is the initial distance between two translation stages and ΔL is the additional displacement when longitudinal stress is introduced to the fibre structure.

Optics EXPRESS

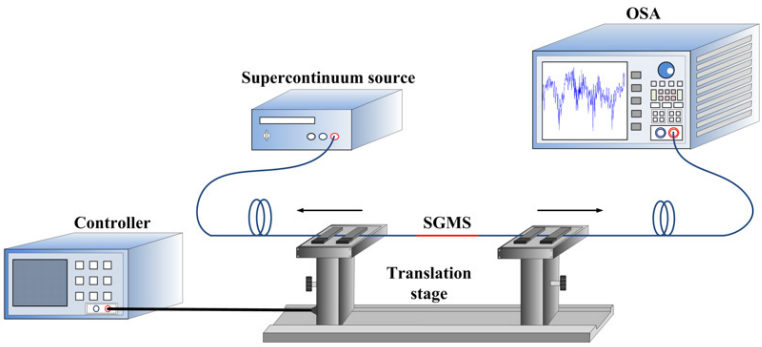

Fig. 5. Experimental setup for the strain measurement using the SGMS fibre structure.

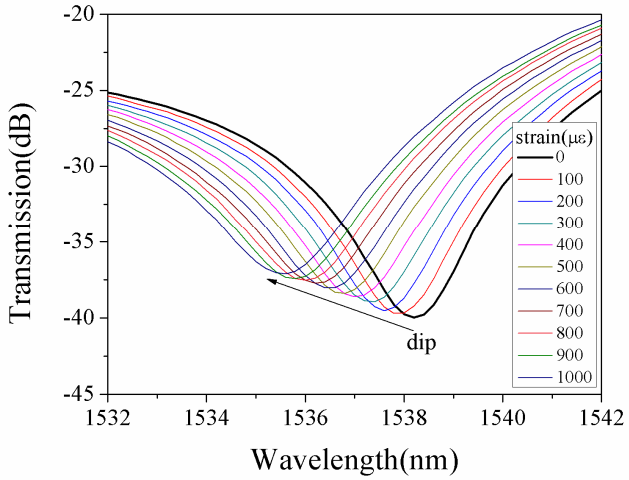

Fig. 6. Transmission spectrum evolution when the applied strain changed.

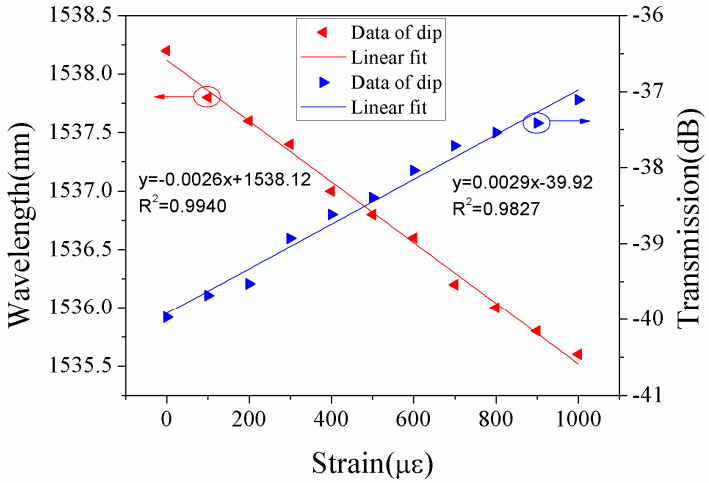

Fig. 7. Dip shift as a function of strain. The red line represents wavelength-strain fitting, the blue line represents intensity-strain fitting.

Optics EXPRESS

The response of the spectral dip centred on the wavelength 1538.2 nm (0 strain) when subject to a strain of up to 1000 με in increments of 100 με is shown in Fig. 6. The spectrum exhibits a clear blue shift accompanied by an intensity increase when the tensile strain was increased from 0 to 1000 με. The resulting change in dip wavelength (red data markers) and value of transmission (blue data markers) versus strain are plotted and fitted in Fig. 7. As shown in Fig. 7, the fitting curve of wavelength-strain (red line) and intensity-strain (blue line) both exhibit a high linear regression coefficient value (R^2) when subject to a linear regression analysis being 0.9940 and 0.9827 respectively. The strain sensitivity of the dip is recorded as −2.60 pm/με and 0.0029 dB/με within the strain range of 0—1000 με, at room temperature of 17.3 °C. To better demonstrate the improved performance for strain sensing of our proposed fiber structure, a comparison experiment based on a standard SMS fiber structure without an F-P cavity was conducted (the length of MMF section is about 2 cm). An appropriate spectral dip centred on a wavelength of 1404 nm was selected and the corresponding transmission spectrum evolution results with increased strain are shown in Fig. 8(a). As was the case in the gourd-shaped SMS fibre structure, a blue shift in wavelength was observed, however, there is no significant intensity change. The corresponding data and fitted results based on wavelength shift compared with gourd-shaped SMS fibre structure are shown in Fig. 8(b). From Fig. 8(b), it is clear that the strain sensitivity of gourd-shaped SMS fibre structure is larger than the standard SMS fibre structure within the same strain range of 0—1000 με. The strain sensitivity of gourd-shaped SMS fibre structure is −2.60 pm/με which is a considerable improvement compared with the strain sensitivity value of −1.60 pm/με for the standard SMS fibre structure.

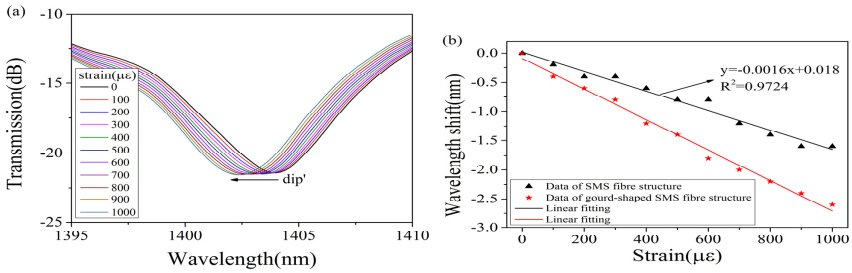

Fig. 8. (a) Transmission spectrum evolution for the standard SMS structure when applied strain is changed; (b) Wavelength shift of a standard SMS fibre structure (triangle points fitted by black line) and the proposed gourd-shaped SMS fibre structure (star points fitted by red line) as a funtion of different strain values.

Table 1 includes a direct comparison with other strain sensors cited in this article. From Table 1, it is clear that the strain sensitivity of the SGMS fibre structure of this investigation is higher than most of the other strain sensors with [19] being the exception of a total of eight cited. As mentioned in Section 1, reference [19] has a clear higher strain sensitivity than the other sensors, but the considerable length of the MMF used in that experiment (up to 1.8 m) makes the sensor physically very long and thus difficult to deploy in many applications. In addition to the strain measurement, the SGMS fibre structure strain sensor has also been investigated for its sensitivity to ambient temperature changes and humidity variations.

Optics EXPRESS

Table 1. Comparison of Different Strain Sensors Developed to Data

Strain sensitivity (pm/με)	Linearity	Temperature-strain cross-sensitivity (με/ °C)	Measurement configuration	Reference number
Not calculated	not given	Not calculated	MMI + FBG	[6]
0.42 ± 5.10-3	not given	16.67	FBG	[13]
−1.5	not given	44.67	LPG	[14]
0.23	0.9996	1.26	Sagnac interferometer	[15]
−1.83	0.9906	39.83	MZI	[16]
2.23	not given	0.14	FPI	[17]
Not calculated	not given	Not calculated	MMI	[18]
18.6	not given	3.12	MMI	[19]
−2.60	0.9940	2.62	MMI + FPI	our work

The temperature dependence and humidity stability of the SGMS fibre structure were measured by placing the sensor in a climate chamber as shown in Fig. 9, in which the temperature and humidity are accurately controlled and the current values of both parameters are shown on an external display panel. Figure 10 shows the spectral output of the SGMS device when subject to a temperature change in the range 30 to 90 °C with an increment of 10 °C and zero strain was applied during the measurements. When the temperature increased, the dip moved to longer wavelengths and the transmission intensity became lower. The dip wavelength and transmission intensity were plotted against temperature in the range 30 to 90 °C and these results are shown in red and blue markers respectively in Fig. 11. Figure 11 also includes a linear fitting, the red line and blue line represent wavelength-temperature and intensity-temperature fitting, respectively. From the linear analysis of Fig. 11, it was determined that the wavelength-temperature sensitivity is 6.8 pm/°C with an R^2 value of 0.9982 and the intensity-temperature sensitivity is −0.0178 dB/°C with an R^2 value of 0.9827. The cross sensitivity between strain and temperature based on wavelength shift is 2.62 με/°C which is competitive with other sensors (Table 1). It is evident that this proposed SGMS fibre structure strain sensor has high strain sensitivity and low temperature-strain cross-sensitivity.

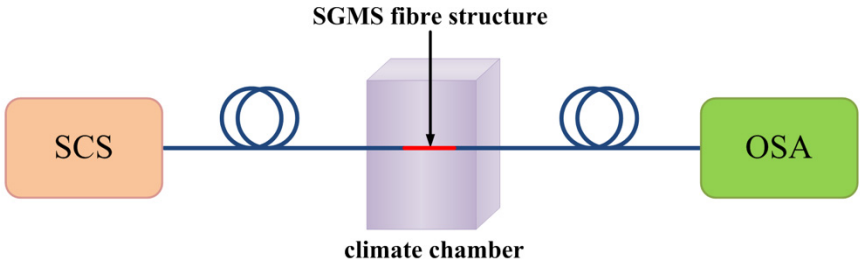

Fig. 9. Schematic diagram of the temperature and humidity measurement setup.

Optics EXPRESS

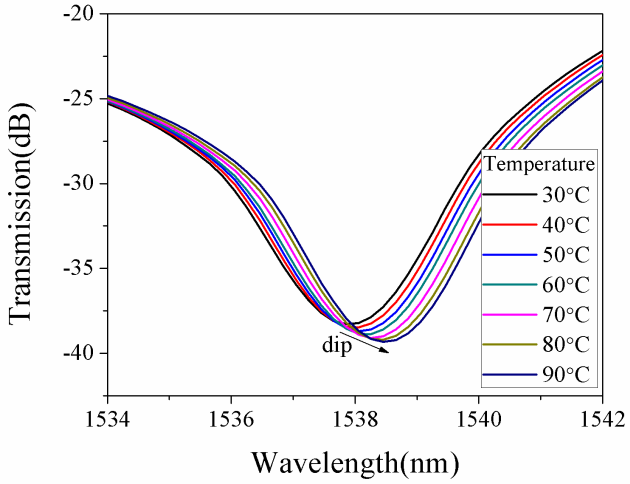

Fig. 10. Transmission spectrum evolution when the surrounding temperature changed.

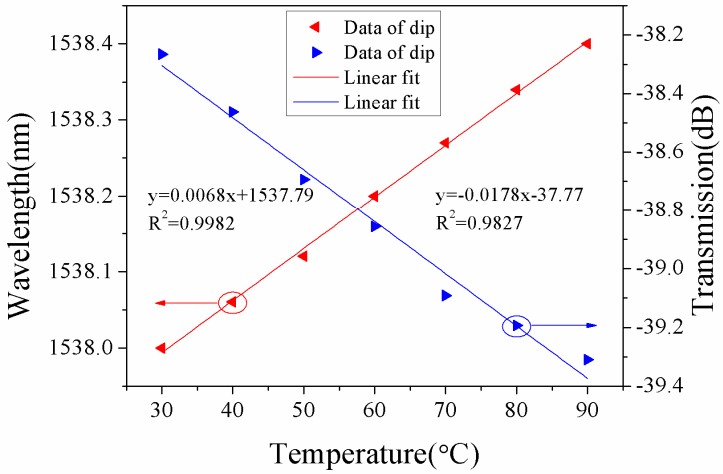

Fig. 11. Dip shift as a function of temperature. The red line represents wavelength-temperature fitting, the blue line represent intensity-temperature fitting.

Based on the strain and temperature sensing characteristics of the SGMS fibre structure, it is feasible that a strain-temperature compensation scheme could be implemented to mitigate temperature effects. A temperature compensation scheme is more feasible if the strain sensitivity is not itself highly dependent on temperature. Thus the strain sensitivity of the dip wavelength of the SGMS fibre structure at different temperatures was also measured and the result is shown in Fig. 12. This figure shows that the strain sensitivity varies in the range –2.54 to –2.72 pm/με over the temperature range from 20 to 70 °C. This represents a change in the strain sensitivity of 0.18 pm/με which is relatively small for such a significant temperature change (50 °C) and the calculated standard deviation σ of the strain sensitivities is 0.069 pm/με. Based on the above results, a direct relationship between strain variation $\Delta\varepsilon$ and temperature variation ΔT can also be determined simultaneously by solving the matrix equation below [27]:

Optics EXPRESS

$$\begin{bmatrix} \Delta\varepsilon \\ \Delta T \end{bmatrix} = \frac{1}{D}\begin{bmatrix} K_{T\Delta P} & -K_{T\Delta\lambda} \\ -K_{\varepsilon\Delta P} & K_{\varepsilon\Delta\lambda} \end{bmatrix}\begin{bmatrix} \Delta\lambda \\ \Delta P \end{bmatrix} \quad (5)$$

where $D = K_{\varepsilon\Delta\lambda}K_{T\Delta P}-K_{\varepsilon\Delta P}K_{T\Delta\lambda}$, and $K_{\varepsilon\Delta\lambda}$, $K_{\varepsilon\Delta P}$, $K_{T\Delta\lambda}$ and $K_{T\Delta P}$ are the strain and temperature sensitivity coefficients which have been determined by the results in Fig. 7 and Fig. 11, respectively. When the ambient temperature is constant, the relationship between the peak wavelength shift and applied strain is linear, as shown in Fig. 6. However, if the temperature changes, the peak wavelength shift varies with the temperature as shown in Fig. 10. Such a wavelength shift also appears as a strain change due to the relationship shown in Fig. 6. The latter can be considered a source of error as it is not a true strain measurement, and can therefore be termed the temperature induced strain error. The calculated result is presented in Fig. 13 which shows the temperature induced strain error in strain measurement. Based on the above analysis and experiments, it can be concluded that implementing temperature compensation in this measurement system is feasible.

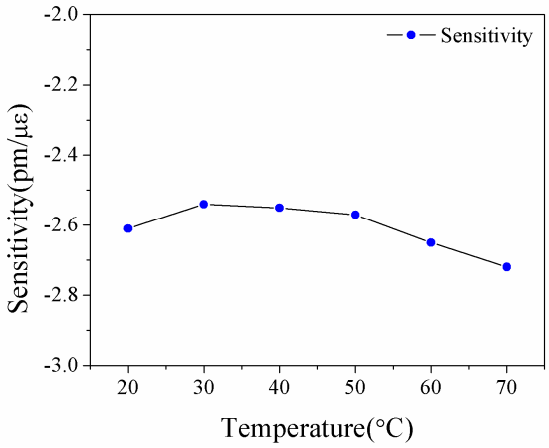

Fig. 12. The wavelength-strain sensitivities of SGMS fibre structure at different temperature.

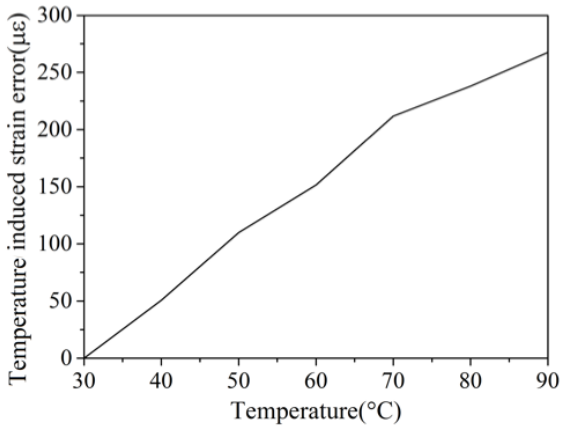

Fig. 13. The temperature induced strain error as a function of temperature.

Finally, the effect of humidity on the structure has also been investigated. Figure 14 shows the spectral response of the SGMS fibre structure to humidity when the relative humidity (RH) was increased from 30% to 90% (at a constant temperature of 30 °C). From Fig. 14, it is clear that there is no significant wavelength shift and the transmitted intensity variation is less

Optics EXPRESS

than 0.307 dB when the environmental humidity is varied as described above. As expected the impact of humidity on the proposed sensor is very low due to the fact that the interference mechanisms are confined internally within the SGMS structure and there is consequently only a negligibly small portion of the evanescent field outside the SGMS fibre structure (as discussed in Section 3).

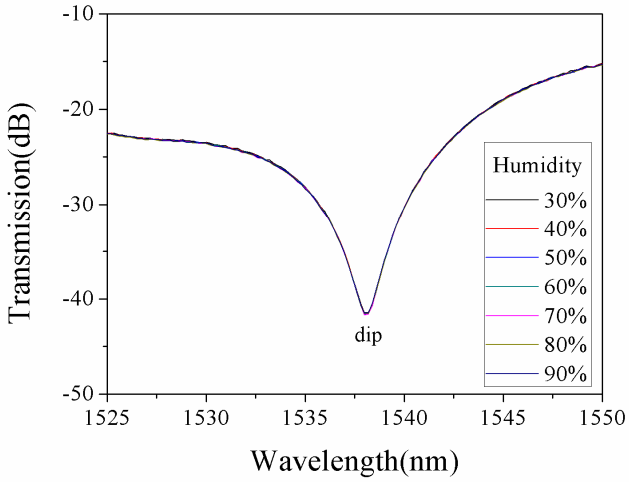

Fig. 14. Dip shift response the surrounding relative humidity change.

5. Conclusion

A fibre-optic strain sensor based on a gourd-shaped joint MMF sandwiched between two SMFs has been successfully fabricated and investigated. The fabrication process is simple and convenient requiring only the use of a standard commercial fusion splicer. The cladding regions at the tip of two MMFs were reshaped to form hemispheres using an electrical arc method and then spliced together to form a gourd shape, but the cores of the MMF fibres remain separated. The gourd-shaped section forms a Fabry-Perot cavity between the two adjacent ends of the multimode fibres. A composite interference pattern based on the inherent multimode interference (MMI) of the MMF and the Fabry-Perot interferometer (FPI) is evident and has been used to demonstrate a significant improvement in the performance compared to a traditional spliced SMS fibre structure. The observed output spectrum shifts in response to the applied strain and resulted in a strain sensitivity of –2.60 pm/με over the range 0—1000 με. Furthermore, the sensor demonstrates experimentally a low temperature dependence for strain sensitivity which is also unaffected by humidity changes.

Funding

Key Program for International S&T Cooperation Projects of China (Ministry of Science and Technology China, Grant no.: 2016YFE0126500), National Natural Science Foundation of China (NSFC, Grant no.: 61575050), Key Program for Natural Science Foundation of Heilongjiang Province of China (Department of Science & Technology of Heilongjiang Province, Grant no.: ZD2016012), 111 project (Ministry of Education China, Grant no.: B13015) at the Harbin Engineering University, and by the Fundamental Research Funds of the Central University (Ministry of Education China) and the Harbin Engineering University.